Exosome-functionalized polyetheretherketone-based implant with immunomodulatory property for enhancing osseointegration

Lei Fan [a,b,1], Pengfei Guan [c,1], Cairong Xiao [a,1], Huiquan Wen [e], Qiyou Wang [c], Can Liu [f], Yian Luo [d], Limin Ma [g], Guoxin Tan [d], Peng Yu [a,*], Lei Zhou [a,d,**], Chengyun Ning [a]

[a] School of Materials Science and Engineering & National Engineering Research Center for Tissue Restoration and Reconstruction, South China University of Technology, Guangzhou, 510641, China
[b] Department of Orthopedic Surgery, Nanfang Hospital, Southern Medical University, Guangzhou, 510515, China
[c] Department of Spine Surgery, the Third Affiliated Hospital of Sun Yat-sen University, Guangzhou, 510630, China
[d] School of Chemical Engineering and Light Industry, Guangdong University of Technology, Guangzhou, 510006, China
[e] Department of Radiology, the Third Affiliated Hospital of Sun Yat-Sen University, Guangzhou, 510630, China
[f] Department of Spine Surgery, the First Hospital of Zhejiang University, Hangzhou, 310003, China
[g] Department of Orthopedics, Guangdong Provincial People's Hospital, Guangdong Academy of Medical Sciences, Guangzhou, 510080, China

ARTICLE INFO

ABSTRACT

The host immune response effecting on biomaterials is critical to determine implant fates and bone regeneration property. Bone marrow stem cells (BMSCs) derived exosomes (Exos) contain multiple biosignal molecules and have been demonstrated to exhibit immunomodulatory functions. Herein, we develop a BMSC-derived Exos–functionalized implant to accelerate bone integration by immunoregulation. BMSC-derived Exos were reversibly incorporated on tannic acid (TA) modified sulfonated polyetheretherketone (SPEEK) via the strong interaction of TA with biomacromolecules. The slowly released Exos from SPEEK can be phagocytosed by co-cultured cells, which could efficiently improve the biocompatibilities of SPEEK. *In vitro* results showed the Exos loaded SPEEK promoted macrophage M2 polarization via the NF-κB pathway to enhance BMSCs osteogenic differentiation. Further *in vivo* rat air-pouch model and rat femoral drilling model assessment of Exos loaded SPEEK revealed efficient macrophage M2 polarization, desirable new bone formation, and satisfactory osseointegration. Thus, BMSC-derived Exos–functionalized implant exerted osteoimmunomodulation effect to promote osteogenesis.

1. Instruction

Healing bone defects using regenerative medicine remains a huge challenge since bone regeneration is a complex mechanism that requires the collaboration of a multitude of specialized cells [1]. Recent studies have deepened our understanding of how immune cells play a vital role in bone regeneration giving rise to a new research field termed "osteoimmunology", suggesting strong crosstalks between immunology and the skeletal system [2]. Traditional bone substitute materials possessed the ability to direct osteoblastic lineage cells osteogenesis *in vitro* which were developed to facilitate bone regeneration. However, some inconsistencies between *in vitro* and *in vivo* experiments were

observed, for instance, materials that were beneficial for *in vitro* osteogenesis cannot promote bone regeneration *in vivo* [3]. Based on the knowledge of osteoimmunology, just emphasizing the direct osteogenesis but ignoring the immune reactions caused by biomaterials is insufficient for researching and developing a new bone biomaterial [2–4]. Hence, a suitable bone biomaterial should not only be able to mediate osteogenesis but also has to be able to manipulate the immune response to exert a synergistic effect for achieving satisfactory osseointegration [5].

The implanted biomaterials are often identified as foreign substances by the host immune system and trigger a cascade of immune responses. Macrophages are identified as important innate immune cells that play

an essential role as effector cells to initiate and maintain inflammation in the immune response [6]. In addition, highly plastic macrophages show polarization states which can switch phenotypes into the pro-inflammatory M1 and anti-inflammatory M2 phenotype [6,7]. The implantation of synthetic biomaterials leads to an activated M1 phenotype that subsequently secretes a large number of pro-inflammatory cytokines, such as interleukin 6 (IL-6), interleukin1β (IL-1β), inducible nitric oxide synthase (iNOS) and tumour necrosis factor alpha (TNF-a) [8]. The prolonged exposure to the pro-inflammatory cytokines eventually leads to chronic inflammation, which induces fibrous encapsulation formation around the implantation materials and finally results in osseointegration failure [9]. The M2 phenotype has a direct role in activating the bone defect regeneration process by secreting anti-inflammatory cytokines, including arginine (Arg-1), interleukin 10 (IL-10) which are beneficial for bone regeneration environment formation [3,9]. Therefore, effective modulation of the macrophage M2 polarization to form a local bone regeneration environment is tightly linked to osteogenic differentiation and osseointegration.

Bone mesenchymal stem cells (BMSCs) with strong immunomodulatory property have been applied in various inflammatory and degenerative diseases [10], as well as in osteoimmunomodulation [11]. Evidence suggests that the direct cell replacement therapeutic effect of BMSCs is limited. BMSCs exert their therapeutic effect primarily through paracrine secretion mechanisms [12]. As carriers of paracrine secretions, BMSC-derived exosomes (Exos) contain multiple biosignal molecules, including protein, lipid and small RNAs that can be transferred to target cells to exhibit the immunomodulatory functions [13,14]. Furthermore, Exos can improve the immunomodulatory capacity by switching macrophages from the M1 phenotype to the M2 phenotype [15]. In addition, Exo-based cell-free therapy can also directly induce the osteogenic differentiation *in vitro* and new bone formation *in vivo* since they contain an abundance of osteogenesis regulation related miRNAs [14,16]. Hence, BMSC-derived Exos with immunomodulatory and osteogenic properties are suitable for bioactive coating on bone substitute materials to stimulate osteogenesis *in vitro*.

In this study, we investigated the BMSC-derived Exos to reversibly immobilize onto a three-dimensional (3D) porous polyetheretherketone (PEEK) surface. PEEK as its good mechanical properties, radiolucency, and chemical resistance, emerged as a substituted implant to replace metal materials in bone engineering [17,18]. After etching using concentrated sulfuric acid, a 3D porous structure was constructed on the PEEK surface which is not only favorable for Exos loading and delivery but also beneficial for improving osseointegration [17,19]. Large amounts of polyphenol groups in tannic acid (TA) can bridge Exos onto underlying PEEK via reversible hydrogen bond, which ensured that the Exos exhibited a sustained release effect. Both *in vitro* RAW264.7 cells/materials co-cultured model and *in vivo* rat air-pouch model were performed to assess the immunomodulatory effect of Exo-coated TA-S-PEEK, which demonstrated that released Exos contained inflammation regulation related miRNAs which can negatively modulate the NF-κB pathway to promote macrophages M2 polarization. Meanwhile, *in vitro* RAW264.7 cells/BMSCs co-cultured model and *in vivo* femoral models were used to evaluate the osteoimmunomodulation of Exo-coated TA-SPEEK, which demonstrated that sustained release Exos from TA-SPEEK can create a suitable immune microenvironment which was beneficial for bone regeneration. In addition, the direct osteogenesis property of Exo-coated SPEEK was also evaluated by exerting BMSCs/materials co-cultured model.

2. Materials and methods

2.1. Rat bone marrow stem cells (BMSCs) and mouse mononuclear macrophage leukemia cells (RAW264.7 cells) obtained

The BMSCs were obtained from bilateral humeri and femurs of

female Sprague Dawley (SD) rat (n = 1; 2-weeks old) by rinsing the bone marrow cavity as described in our previous studies [20]. Obtained cells were cultured in Dulbecco's modification of Eagle's medium Dulbecco (DMEM, GIBCO) medium containing 10% fetal bovine serum (FBS, GIBCO) at 37 °C with 5% CO2. RAW264.7 cells were purchased from ATCC cell bank and cultured in 1640 medium (GIBCO) at 37 °C with 5% CO2

2.2. Isolation and characterization of BMSC-derived Exos

Firstly, the Exo-free FBS was prepared by ultracentrifuging at 120000 g under 4 °C for 14 h in an ultracentrifuge (Optima-90 K, Beckman Coulter) for further BMSCs culture. The BMSCs medium was collected 48 h after cultured and subsequently underwent multistep centrifugation at 2000 g for 20 min, followed by 10000 g for 30 min, and finally, 100000 g for 90 min to separate Exos (Fig. S1a). Transmission electron microscopy (TEM, HT7700, HITACHI), qNano® system (Izon Science), and Western blot were performed to verify the morphology, particle size, and the surface marker including CD9 (ProteinTech), CD63 (ProteinTech), and TSG101 (Abcam) of Exos, respectively.

2.3. BMSC-derived Exos labeling

Exos were marked with PKH26 red fluorescent dye (Sigma-Aldrich). Exos from 10×10^8 cells were resuspended in 100 μL phosphate buffered saline (PBS, GIBCO) and incubated in PKH67 which diluted in 20 μL Diluent C at the concentration of 1:50. After incubation at room temperature for 5 min, an equal volume of Exo-free medium was dripped in to terminate the labeling reaction. Finally, Exos were re-obtained by centrifugation at 100000 g for 1 h to remove unbound dye solution.

2.4. Sample preparation

A PEEK disc of 2 cm in diameter was used for the *in vitro* experiments and subcutaneous implantation (Fig. S2a). A PEEK disc of 1 cm in diameter was used for the material science testing and subcutaneous implantation (Fig. S2b). A PEEK stick of 1.8 mm in diameter and 0.8 cm in length was used for the femur implantation (Fig. S2c). PEEK was immersed into 95–98 wt% sulfuric acid solution (Aldrich Chemical Corp) and stirred for 2 min to form a uniform porous structure. The sulfonated-PEEK (SPEEK) then underwent hydrothermal treatment (120 °C, 6 h) to remove residual sulfuric acid. The SPEEK were subsequently soaked in 40 mL solution following final concentrations (FeCl3 6H2O: 0.1 mg/mL, TA: 0.4 mg/mL). Subsequently, the pH of this solution was raised to 8 by dripping 1 N NaOH solution and reacted with samples under magnetic stirring conditions for 10 s to obtain TA-SPEEK. Afterward, PBS was used to repeatedly rinse the obtained samples to remove unpolymerized monomer. 127.39 μg/cm² BMSC-derived Exos were finally dripped onto the TA-SPEEK and cocultured under 4 °C for 24 h to synthesize the Exo-TA-SPEEK sample.

2.5. Surface characterization

The surface morphology of each sample was scanned by field-emission scanning electron microscopy (FE-SEM, ZEISS) and atomic force microscopy (AFM, Bruker). The surface roughness measurement was characterized by the surface Roughness Tester (TR200). Fourier transform infrared (FTIR, Nicolet6700, Thermo Fisher) was employed to perform the surface chemical composition analysis. Contact angle was measured to evaluate the surface hydrophilicity of each sample by using a contact angle meter (SL200B). The PKH26 (Sigma) labeled Exos were confirmed to bind onto the surface of the TA-SPEEK by using a confocal laser scanning microscopy (Leica).

2.6. Exos release and phagocytosis

To investigate the optimal concentration of Exos loaded on the TA-SPEEK, varying amounts of Exos (63.69 µg/cm^2, 127.39 µg/cm^2, 191.08 µg/cm^2) were dripped onto the TA-SPEEK. The amount of Exos in the supernatant was detected immediately after Exo-TA-SPEEK immersed into the medium. The total amount of Exos minus the Exos in the supernatant is the amount of loaded Exos. Three repeat samples were dropped into 2 mL serum-free medium and cultured for 0, 1, 3, 7, and 14 days at 37 °C to investigate the Exos release property of Exo-loaded SPEEK. At each timepoint, the medium was replaced and 100 µl supernatant was diverted into a 96-well plate to detect the concentration of released Exos by using a bicinchoninic acid (BCA) reagent test kit (Thermo Scientific). Exos release property was also evaluated in an acidic environment (PH 6.5) to mimic the inflammation state *in vivo*. The daily Exos release was expressed as concentration per effective surface area. The cumulative Exos release was calculated by the total amount of release Exos compared with the total amount of added Exos. After RAW264.7 cells and BMSCs cultured on the Exos (PKH26-labeled) loaded TA-SPEEK for 24 h, 4% paraformaldehyde was used to fixed the cells which subsequently underwent cytoskeleton staining (phalloidin-Alexa Fluor, Beyotime) to analyze the phagocytosis of released Exos.

2.7. In vitro studies

2.7.1. In vitro biocompatibility of samples

The live/dead analysis, Cell counting kit-8 (CCK-8, Dojindo), and cytoskeletal staining were used to analyze the *in vitro* biocompatibility of each sample. Calcein-AM/ethidium (CalceinAM/PI, Invitrogen) was used to evaluate the viability of 5×10^5 BMSCs and 5×10^5 RAW264.7 cells one day after they were cultured on each sample in 12-well plate. 2 µM Calcein-AM and 4.5 µM PI was added to the culture medium to incubate with BMSCs for 20 min at 37 °C in 5% CO$_2$. The micrographs were captured by a confocal reflection microscope (Leica). The proliferation of BMSCs and RAW264.7 cells was evaluated by CCK-8 solution after 5×10^5 cells were cultured on each sample in 12-well plate for 1 day, 3 days, and 7 days. CCK-8 solution was added to 12-well BMSCs/sample co-culture plates at the concentration of 100 µl/ml. After incubation for 2 h, 100 µL supernatant was transferred into 96-well plates and the optical density (OD) values were evaluated by an enzyme-labeling instrument (BioTech) at 450 nm wavelength. After 2.5×10^5 BMSCs were cultured on each sample in an 12-well plate for 3 days and 1×10^5 RAW264.7 cells were cultured on each sample in an 12-well plate for 3 days and 7 days, the cytoskeleton was stained with phalloidin-Alexa Fluor. Then the micrographs were captured by a laser confocal scanning microscope (Leica).

2.7.2. Osteoimmunomodulation effects on BMSCs

To evaluate the osteoimmune environment effect on the osteogenic differentiation of BMSCs, an Exo-loaded SPEEK/RAW264.7 cells/BMSCs co-cultivation model was established. As Fig. 4a showed, 1×10^5 RAW264.7 cells were cultured on the samples and placed on the lower plate, and 1×10^4 BMSCs were cultured in the transwell chamber. A polycarbonate membrane with 1.0 µm pore size was used to isolate the two cell types but cytokine exchange was allowed.

2.7.3. Alkaline phosphatase (ALP) staining and quantification

A 5-bromo-4-chloro-3-indolyl phosphate/Nitro blue tetrazolium (BCIP/NBT) ALP color development kit (Beyotime) and ALP assay kit (Beyotime) was used to stain and quantify the ALP activity of BMSCs, respectively. After BMSCs were fixed in 4% paraformaldehyde for 30 min, pre-prepared BCIP/NBT dyeing was added and incubated with samples for 1 h to stain ALP. BCIP/NBT dyeing was removed and rinsed by distilled water to terminate the staining reaction. The images of ALP staining were captured by a digital camera (Canon). For ALP quantification, BMSCs were lysed by using 1% v/v Triton X-100 (Biofroxx) on ice for 30 min. The cell-lysis solution was centrifuged for 30 min at 12000 rpm under 4 °C and then the supernatant was collected. Afterward, 50 µL supernatant was mixed with equal volume ALP assay working solution and incubated for another 30 min. The ALP activity was measured at 405 nm wavelength by using an enzyme-labeling instrument (BioTech).

2.7.4. Alizarin red S (ARS) staining and quantification

ARS staining was used to measure the property of mineralized nodule formation. Briefly, BMSCs were fixed in 75% ethanol for 1 h. Afterward, 2% ARS solution (pH 4.2, Sigma–Aldrich) was dripped onto the samples and incubated for 10 min. Unreacted ARS was rinsed thoroughly using distilled water. The images of deposited calcium were captured by a digital camera (Canon). Then the stained samples were soaked into 1 w/v% hexadecylpyridinium chloride (Merck) for 1 h under shaking condition. 100 µl suspension was transferred into 96-well plates and quantified at 570 nm wavelength by an enzyme-labeling instrument (BioTech).

2.7.5. TRAP staining

1×10^5 RAW264.7 cells were incubated in a TRAP staining kit (BestBio) after culture for 1 and 7 days. Briefly, the cells were fixed in TRAP fixative for 1 min and then stained in TRAP incubation solution for 50 min. After washing three times, samples were stained with hematoxylin staining solution for 5 min. Finally, the images of TRAP staining were captured by a digital camera (Canon).

2.7.6. Gene expression

The total mRNA was harvested by total RNA kit (Omega) and reversely transcribed into cDNA by using a reverse transcription kit (Takara). Real-time qPCR (RT-qPCR) was performed with LightCycler 480 SYBR Green I Master (Roche) and implemented by using the LightCycler® 480II (Roche). This assay was repeated in triplicates and quantitatively calculated by using the $2^{-\Delta\Delta Ct}$ method. The primers of each gene are listed in Table S1.

2.7.7. Immunofluorescence analysis

Cells or tissues were fixed in 4% paraformaldehyde for 30 min, and then permeabilized using 0.2% Triton X-100 (Biofroxx) for 1 h at room temperature. After blocking in 3% bovine serum albumin (BSA, Biofroxx) for 1 h, corresponding primary antibodies (Table S2) proportionally diluted in 3% BSA were added for incubation at 4 °C overnight. Corresponding secondary antibodies were added to combine with the primary antibody for 1 h. Finally, Nuclei were stained by Hoechst (Sigma) for 5 min the micrographs were captured by using a confocal reflection microscope (Leica).

2.7.8. Western blot assay

Cells or tissues were lysed in radio-immunoprecipitation assay (RIPA) lysis buffer (CWBIO) with phosphatase and protease inhibitors (Thermo Fisher) on ice for 30 min. The concentration of each protein was measured by using a BCA protein assay kit. After protein denaturation by heating at 100 °C for 10 min, 40 µg protein suspension was loaded on SDS-PAGE gels for gel electrophoresis to separate proteins, and subsequently transferred onto polyvinylidenefuloride (PVDF, Thermo Fisher) membranes. The membranes were blocked in 5% skimmed milk for 1 h and then incubated with the primary antibodies overnight at 4 °C. After incubation using secondary antibodies (CST) for 1 h, an enhanced chemiluminescence (ECL) kit was used to visualize immunoblots. ImageJ software was used to quantitatively analyze the density of each protein band.

2.8. In vivo studies

2.8.1. Ethics statement

Animal experiments were approved by the Animal Care and

Experiment Committee of South China Agricultural University. Animal maintenance and all experimental procedures were done in accordance with the National Institutes of Health Guide for the Care and Use of Laboratory Animals.

2.8.2. Rat air-pouch model

Twelve eight-week-old female SD rats were assigned into four groups (PEEK group, SPEEK group, TA-SPEEK group, and Exo-TA-SPEEK group, n = 3). Briefly, 10 mL sterile air was subcutaneously injected into the back of the rat to form a dorsal air-pouch. Three days and six days later, 5 mL sterile air was reinjected to maintain the air-pouches, respectively. Rats were anesthetized by intraperitoneal injection of 6 mg/kg xylazine and 70 mg/kg ketamine seven days later following the formation of a stable air-pouch. After the skin above the air-pouch was shaved and disinfected, a 1 cm incision was created at the edge of the air-pouch to implant each sample. The incision was sutured and disinfected subsequently.

2.8.3. Rat femoral model

Twelve eight-week-old female SD rats were assigned into four groups (PEEK group, SPEEK group, TA-SPEEK group, and Exo-TA-SPEEK group, n = 3). Xylazine (6 mg/kg) and ketamine (70 mg/kg) were intraperitoneally injected to anaesthetize each rat. The left leg was shaved and sterilized thoroughly using povidone iodine. The femoral condyle was exposed by cutting the medial patellar skin and muscles under a sterile condition. Afterward, a 2 mm diameter hole was drilled along the longitudinal axis of the femur through the femoral condyle using a 15 G needle. After each sample was inserted into the prepared holes, the incision was sutured and disinfected again. The rats were then housed in separate cages and allowed to freely obtain food and water. All rats were euthanized at 8 weeks postoperatively.

2.8.4. Microcomputed tomography (Micro-CT) evaluation

The rats were sacrificed by carbon dioxide asphyxiation to obtain the femur. *In vivo* new bone formation induced by implants was observed by a Micro-CT device (LCT-200, Aloka) at 8 weeks. The 2D and new bone reconstructed 3D models were analyzed by Latheta v3.61 software. The grey threshold value used for newly formed bone analysis was Hu value from 650 to 1800. The bone volume/total volume (BV/TV), bone mineral density (BMD), trabecular number (Tb.N), trabecular thickness (Tb. Th), and trabecular separation (Tb.Sp) was quantitatively calculated using Analyze 14.0 software.

2.8.5. Histological evaluation

7 days after samples implantation, animals were sacrificed by carbon dioxide asphyxiation. The skin tissues surrounding the samples were removed and fixed in 4% paraformaldehyde for 3 days. After the tissue samples gradient dehydrated, they were embedded in paraffin and sectioned by a Leica RM2245 electric slicer. Sections were stained by Hematoxylin & Eosin (HE) stain and Masson Trichome stain for general thickness analysis of the inflammation layer and collagen evaluation respectively. Rat femurs were fixed in 4% paraformaldehyde for 3 days and subsequently dehydrated in graded ethanol to change the tissue from the aqueous stage to the organic stage. After embedding samples in methylmethacrylate (Tokyo Chemical Industry), they were cut into sections with a thickness of 200 μm using a slicer (EXAKT CP300), and then grinded into sections 15-20 μm thick using a grinding machine (EXAKT CS400). Afterward, the sectioned samples were stained with methylene blue/acid fuchsin (Merck) stain and observed using an optical microscope (OLYMPUS CX43). The length of the bone in contact with the implant was determined according to the histological image.

2.8.6. Statistical analysis

At least three samples were used in each group, and the results were shown as mean ± standard deviations (SD). Statistical product and service solutions software (SPSS, version 22.0) was used for the statistical analyses. One-way analysis of variance (ANOVA) followed by Bonferroni's multiple comparison test was used to measure the statistically significant difference (p) among groups, and a p-value < 0.05 was recognized as a difference.

3. Results and discussion

3.1. Production and characterization of Exos

The process of Exos production was showed in Fig. S1a. TEM images revealed that the obtained spherical particles exhibited a cup-shaped morphology (Fig. S1b). The size of spherical nanoparticles was around 97.6 ± 50.2 nm as showed by the qNano® system, which was consistent with the size of TEM analysis (Fig. S1c). Western blot analysis displayed a significant increase in surface markers, including CD9, CD63, and TSG101 proteins on the obtained nanoparticles when compared to BMSCs (Fig. S1cd). Together, these results confirmed that the BMSC-derived Exos were successfully obtained.

3.2. Characterizations of materials

Samples preparation is showed in Fig. 1a. The surface morphology of samples was detected by FE-SEM and AFM images (Fig. 1b and c). After PEEK was treated by sulfuric acid, a 3D network porous morphology structure replaced the originally smooth structure (Fig. 1b). Sulfonation is an effective and common way to fabricate a porous structure on PEEK. As previous reported that Gel permeation chromatography analysis revealed no significant differences in apparent molecular weights between the samples with or without sulfonation [21,22]. The molecular weights of PEEK before and after sulfuric acid treatment was around 100000 g/mol [22].The pore size was similar to previous studies that reported pores between 0.5 and 2.0 μm in diameter which was favorable for delivery of biological factors [22–24]. Meanwhile, the surface roughness of SPEEK was significantly increased from (Ra = 0.05 ± 0.02 μm) to (Ra = 1.50 ± 0.15 μm) (Fig. S3a). SPEEK was then dipped into Fe^{3+} and TA solutions to form the TA layer through hydrogen bonding. The pH of the solution was also kept at 8 to maximize the interactions [25]. TA molecule with high content of trihydroxyphenyl and dihydroxyphenyl anchor groups has attracted widespread attention in surface engineering [26]. Fe^{3+} can interact with up to three 3, 4-dihydroxy-L-phenylalanine (DOPA) catechol functionalities to promote TA crosslinking [27]. As numerous TA nanoparticles dopped into SPEEK, a Fe^{3+}-TA particulate film formed into the porous structure of SPEEK (Fig. 1b). The surface roughness was increased (Ra = 1.86 ± 0.20 nm) but showed no obvious difference when compared to SPEEK (Fig. S3a). Furthermore, an Exos containing solution was dripped onto the TA-SPEEK. As FE-SEM, AFM and immunofluorescence images show, densely and uniform Exos were deposited onto the TA-SPEEK surface (Fig. 1b, c, d). Interestingly, the varying amounts (63.69 μg/cm², 127.39 μg/cm², 191.08 μg/cm²) of loaded Exos all exhibited continuous and slow release from the TA-SPEEK for up to 14 days (Fig. S3b). However, the amount of released Exos was significantly higher in 127.39 μg/cm² and 191.08 μg/cm² groups when compared to 63.69 μg/cm² group in each timepoint. 68.37 ± 3.89 μg/cm² Exos was released immediately after Exo-TA-SPEEK immersed into the medium in the 191.08 μg/cm² group. The daily Exos release curve of the 191.08 μg/cm² group almost coincided with the 127.39 μg/cm² group from day 1 and onwards, indicating that adding an increased amount of Exos does not increase its effective load concentration. The number of hydrogen bonds in tannic acid limited the graft of Exos (Fig. S3b). Meanwhile, the Exos released from the SPEEK exhibited a significant aggregation in the first three days when compared to those released from the TA-SPEEK (Fig. 1e and f). As Fig. S3c also showed that the amount of Exos loaded on the samples exhibited continuous decrease over time. IF image showed that almost no Exos remained on the sample surface14 days after initial release. In addition, Exos also showed continuous and
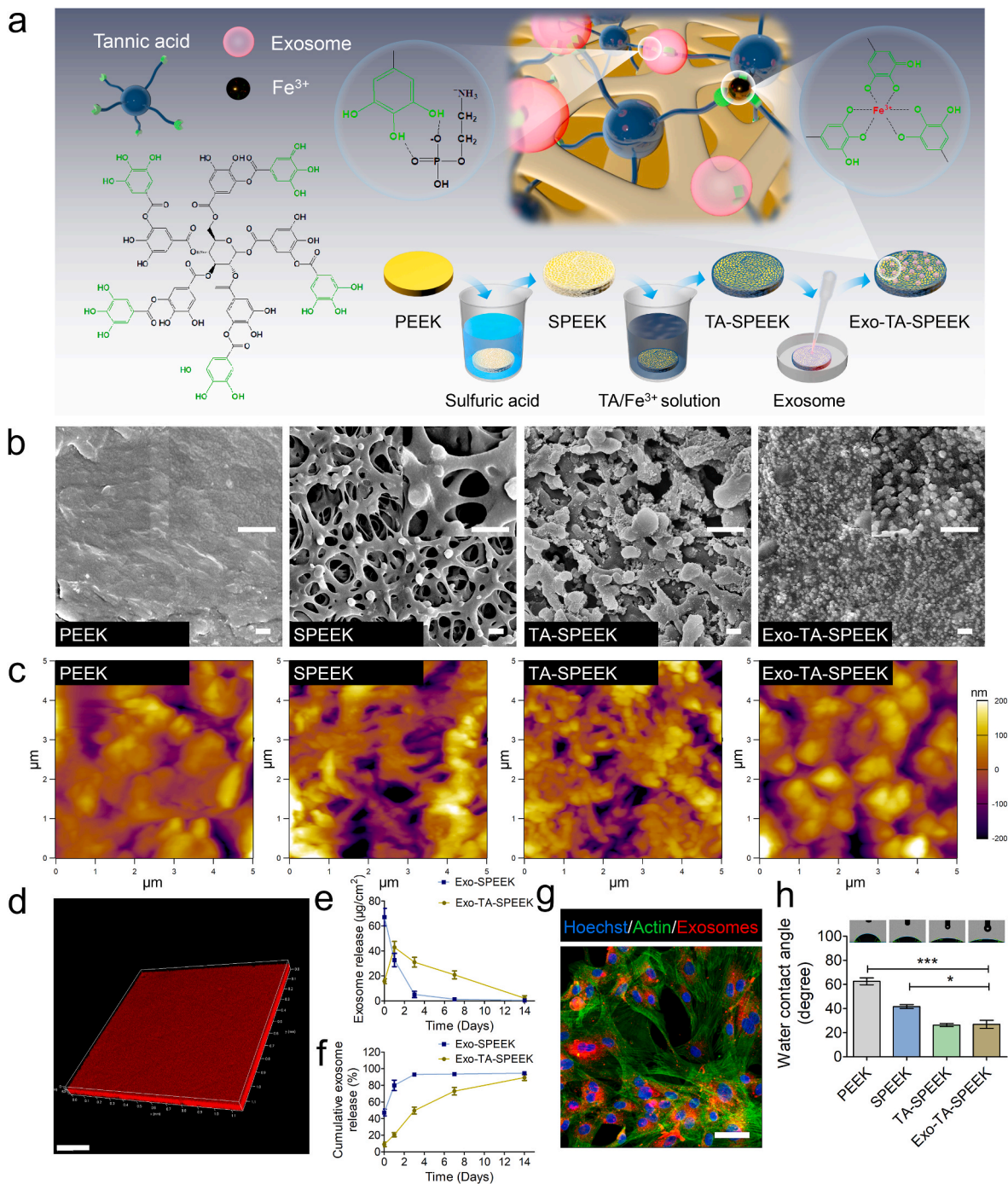
Fig. 1. Characteristics of different samples. (a) Illustration of surface modification of PEEK. Fe^{3+} acts as an ionic cross-linker that can interact with up to three 3,4-dihydroxy-ʟ-phenylalanine (DOPA) catechol functionalities to promote TA crosslinking. BMSC-derived Exos were reversibly bound to TA-SPEEK via hydrogen bond formation between phosphate groups in Exos phospholipid and polyphenol groups in the TA molecule. (b) FE-SEM images of PEEK, SPEEK, TA-SPEEK and Exo-TA-SPEEK. Scale bar represents 500 nm. (c) AFM images of PEEK, SPEEK, TA-SPEEK and Exo-TA-SPEEK. (d) 3D immunofluorescence images show an even distribution of Exos on the TA-SPEEK surface. Scale bar represents 200 μm. (e) The daily Exos released from SPEEK and TA-SPEEK within 14 days (n = 3). (f) Cumulative Exos release curve of SPEEK and TA-SPEEK up to 14 days (n = 3). (g) Immunofluorescence images show PKH26 labeled Exos were phagocytized by the BMSCs. Scale bar represents 200 μm. (h) Water contact angles of each sample (n = 3). ANOVA followed by Bonferroni's multiple comparison test was used for statistical analysis (*p < 0.05, **p < 0.01, ***p < 0.001).

slow release properties in an acidic environment (PH 6.5, Fig. S3d). The cumulative Exos release curve showed that nearly 90% of the Exos were release from both SPEEK and TA-SPEEK *in vitro* (Fig. 1f). The difference is that the time to reach the release equilibrium, in SPEEK was 3 days while it was 14 days in TA-SPEEK (Fig. 1f). These results demonstrate that TA is a suitable choice for achieving stable and sustainable Exos release, mainly due to the fact that Exos can reversibly bind to TA-SPEEK

via hydrogen bond formation between phosphate groups in Exos membrane and polyphenol groups in the TA molecule [28,29]. Also, this natural cell membrane of Exos could lead to a series of BMSC–relevant functions such as immune escape and prolonged circulation [30–32]. The sustained release of Exos loaded on TA-SPEEK ensured biomaterials have a more effective therapeutic effect. To investigate whether the process of implant placement could lead to disruption of loaded

exosomes, we took out the implants immediately after placement and observed the cumulative Exos release curve. As shown in Fig. S3e, more than 80% of the Exos were released from Exo-TA-SPEEK, suggesting that the process of implant placement did not obviously damage the loaded exosomes (Fig. S3e). In addition, the Exos released from TA-SPEEK can be normally phagocytized by the BMSCs (Fig. 1g). The hydrophilic property of each sample was estimated by the water contact angle (Fig. 1h). The contact angle of SPEEK was significantly reduced to 41.63 ± 2.66° when compared to PEEK (62.53 ± 5.00°), indicating that a rough surface morphology becomes more hydrophilic [33]. After hydrophilic TA molecular dropped onto SPEKK, the contact angle was further reduced from 41.63 ± 2.66° to 26.27 ± 2.14°. No significant difference was detected between the TA-SPEEK (26.27 ± 2.14°) and Exo-coated TA-SPEEK (26.87 ± 5.75°), which indicated that additional Exos did not significantly change the contact angle. Fig. S3f shows FTIR spectra of PEEK, SPEEK, TA-SPEEK and Exo-TA-SPEEK membranes. In comparison with PEEK and SPEEK substrate, the TA-SPEEK has stretching vibration peaks of hydroxyl groups (single bond-OH) and carbonyl groups (C=O) at ~3374 cm^{-1} and ~1705 cm^{-1}, respectively, which indicated that TA was successfully grafted onto the surface of SPEEK. Moreover, the Exo-TA-SPEEK showed stretching vibration peaks of hydroxyl groups at ~3284 cm^{-1}, but stretching vibration peaks of the carboxyl group was not observed. Concealing the characteristic peaks of the carbonyl group of TA and more prominently reflecting on the characteristic of the hydroxyl group peaks suggested a successfully

loading of Exos onto the surface of TA-SPEEK.

3.3. In vitro biocompatibility of Exo-coated TA-SPEEK

This study aimed to investigate the effect of samples on RAW264.7 cells, we hence seeded RAW264.7 cells on each sample and analyzed the *in vitro* biocompatibility. Meanwhile, since BMSCs proliferation and adhesion are also fundamental to *in vivo* tissue reconstruction [19]. Herein, BMSCs were also seeded on each sample to analyze the *in vitro* biocompatibility of samples. The proportion of living and dead cells was evaluated by staining BMSCs and RAW264.7 with CalceinAM/PI 24 h after culture. Few dead cells were detected on the surface of each sample, which indicated there were no cytotoxic effects caused by the surface of any sample (Fig. 2a-b, and Figs. S4a–b). The proliferation of BMSCs and RAW264.7 cells on samples was evaluated by CCK-8. The results revealed that cell viability of BMSCs or RAW264.7 cells on the Exo-coated TA-SPEEK was significantly higher compared to the other four groups starting from the third day following culture (Fig. 2c and Fig. S4c), which indicated that BMSC-derived Exos on the sample can interact with BMSCs and RAW264.7 cells to rapidly promote cells proliferation [34]. BMSC-derived Exos have been demonstrated to induce rapid phosphorylation of extracellular regulated protein kinase (ERK) and protein kinase B (AKT) pathway which plays an essential role in promoting cell proliferation and migration [35]. The actin-tracker green and Hoechst were used to stain cytoskeleton and cell nuclei of BMSCs 3
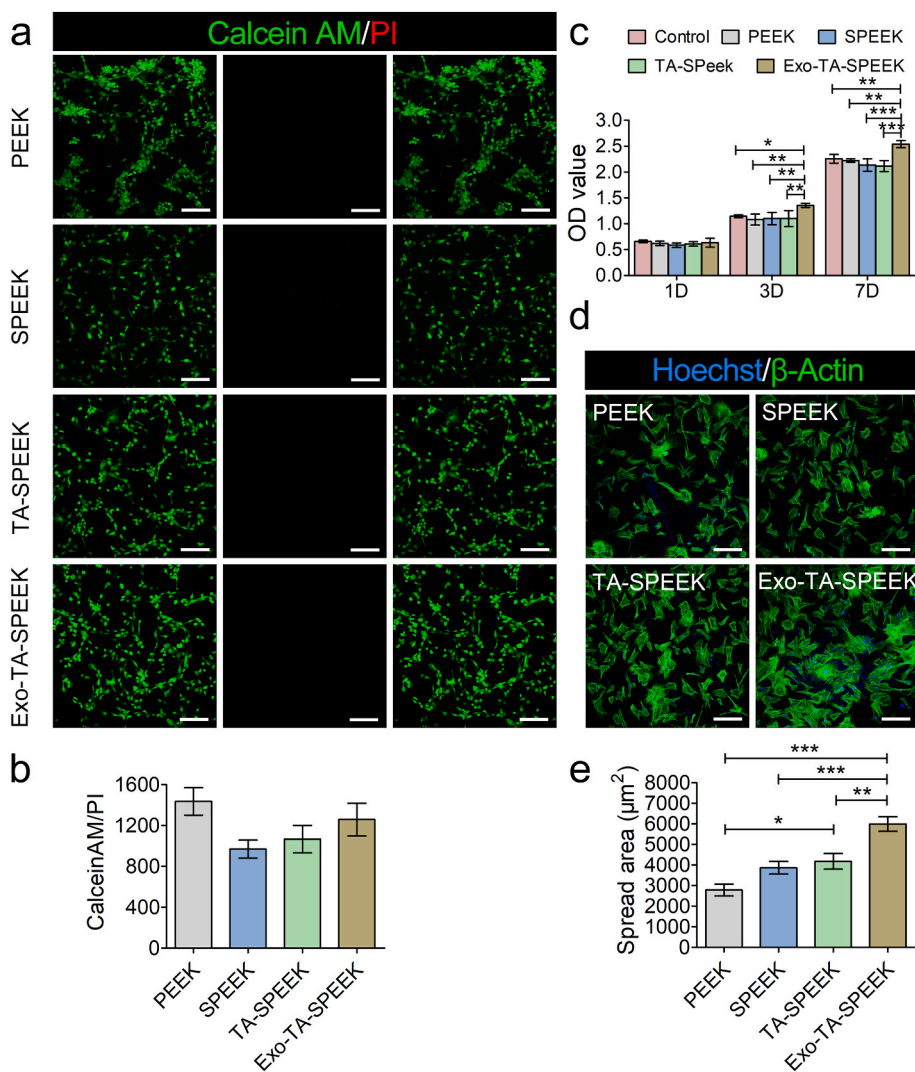
Fig. 2. Biocompatibility of each sample. (a) Live/dead assay of BMSCs cultured on each sample surface for 1 day. The red staining indicated dead cells and green staining indicated live cells. Scale bar represents 100 μm. (b) Quantitative analysis of live/dead assay (n = 3). (c) CCK8 assay was used to evaluate the proliferation of BMSCs cultured on the surface of each sample for 1, 3 and 7 days (n = 5). (d) Immunofluorescence images showed the adhesion of BMSCs cultured on each sample after 3 days following culture. The green staining indicated cytoskeleton and the blue staining indicated nuclei. Scale bar represents 200 μm. (e) Quantitative analysis of cell spread area (n = 9). ANOVA followed by Bonferroni's multiple comparison test was used for statistical analysis (*p < 0.05, **p < 0.01, ***p < 0.001).

days after being cultured on different samples. As shown in Fig. 2d and e, BMSCs stretched better and even interconnected with each other on Exo-coated TA-SPEEK when compared to that on the PEEK, SPEEK, and TA-SPEEK, which indicated a better cell adhesion-enhancing property of Exo-coated TA-SPEEK. In addition, BMSCs cultured on TA-SPEEK showed a more spread morphology when compared to SPEEK and PEEK, indicating that the porous surface and hydrophilic properties of TA-SPEEK were beneficial for cell adhesion [2].

3.4. Acute inflammatory response of RAW264.7 cells

As shown in Fig. 3a, the pro-inflammatory cytokines such as TNF-α and iNOS are considered as the M1 phenotype markers, while the anti-inflammatory cytokines such as Arg-1 and IL-10 are referred to as the M2 phenotype markers [33]. BMSC-derived Exos released from TA-SPEEK can be phagocytized by RAW264.7 cells to exert immunomodulatory function (Fig. 3b). RAW264.7 cells were incubated with lipopolysaccharide (LPS) to induced inflammatory conditions before each experiment. The gene expression, immunofluorescence staining and Western blot analysis were used to assess the inflammation regulation function of each sample after RAW264.7 cells were cultured on samples for 3 days. As RT-qPCR and immunofluorescence result show, the Arg-1 and IL-10 gene and the percentage of Arg-1-positive cells were lower while the iNOS and TNF-α gene and the percentage of iNOS-positive cells were higher in PEEK group when compared to the control and SPEEK group (Fig. 3c–g), which indicated that PEEK, as an exogenous implant, can activate the majority of macrophages polarization from M0 to M1 phenotype to induce detrimental host immune response. However, the

difference between PEEK and SPEEK groups showed no significance. As previously reported, the interactions between material surfaces and cells were important for cellular functions and behaviors [36]. However, the most effective surface modification method was the nanostructure formation which has been used to modulate wettability, surface asperity, and matrix elastic modulus of bone biomaterials to give it osteoimmunomodulatory properties [5,8]. Hence, the immunomodulatory function of the additional porous structure of SPEEK was not obvious which is consistent with previous researches [2,37]. With the addition of TA, TA-SPEEK promoted the gene expression of M2 surface markers (Arg-1 and IL-10), but suppressed the gene expression of M1 surface markers (TNF-α and iNOS) when compared to that of the SPEEK group, which would suggest that TA-SPEEK has an anti-inflammatory effect (Fig. 3c). TA molecular with good antioxidant and anti-inflammatory capacities can moderate immunity [38]. The RAW264.7 cells culture on the Exo-coated TA-SPEEK significantly inhibited the TNF-α gene and iNOS gene, simultaneously promoted Arg-1 gene and IL-10 gene expression from LPS-activated RAW264.7 cells when compared to the other four groups (Fig. 3c). Similarly, cells on the Exo-coated SPEEK group featured a higher percentage of Arg-1-positive cells and a lower percentage of iNOS-positive cells than other groups (Fig. 3d–g). Western blot analysis further verified that Exo-coated SPEEK inhibited the iNOS expression while promoting Arg −1 expression when compared to the other four groups (Fig. 3h and i). All these results suggested that Exo-loaded TA-SPEEK can promote macrophages M2 polarization. Exos are nanoparticles ranging from 30 to 100 nm in diameter which are widely recognized as intercellular messengers, especially in immunomodulation [12]. Plenty of signal molecules including proteins, mRNA, and
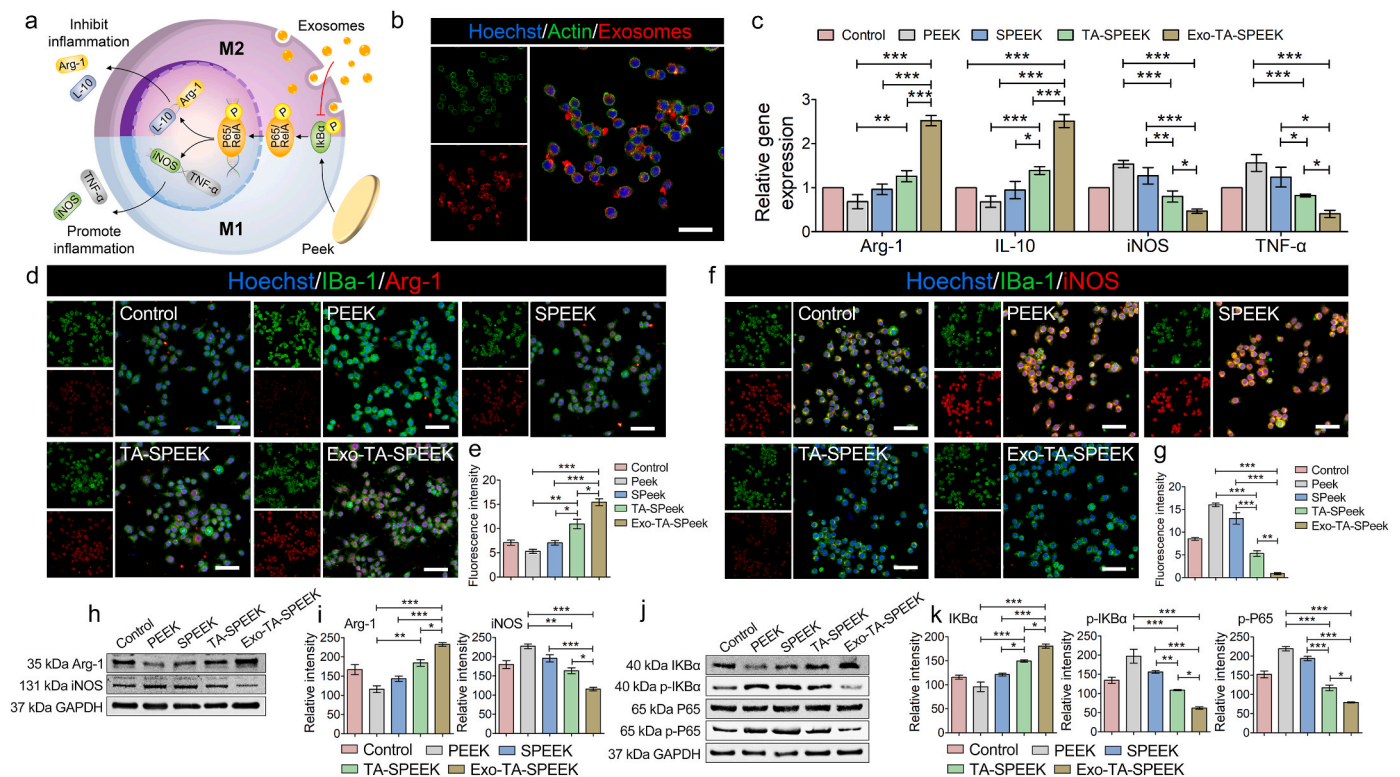
Fig. 3. *In vitro* RAW264.7 cells polarization. (a) An illustration of Exos loaded TA-SPEEK modulating macrophage polarization. (b) Immunofluorescence images show PKH26 labeled Exos phagocytized by RAW264.7 cells. Scale bar represents 50 μm (c) Effects of each sample on the expression of anti- and pro-inflammatory genes were evaluated by RT-qPCR (n = 3). (d) IBa-1 and Arg-1 immunofluorescent staining of RAW264.7 cells on each sample surface are shown three days following culture. IBa-1 was stained green, Arg-1 was stained red and nuclei was stained blue. Scale bar represents 50 μm. (e) Quantitative analysis of immunofluorescent staining (n = 3). (f) IBa-1 and iNOS immunofluorescent staining of RAW264.7 cells on each sample surface three days after culture. IBa-1 was stained green, iNOS was stained red and nuclei was stained blue. Scale bar represents 50 μm. (g) Quantitative analysis of immunofluorescent staining (n = 3). (h) Western blot analysis of Arg-1 and iNOS protein expression. (i) Quantitative analysis of Western blot (n = 3). (j) Western blot analysis of protein expression (IKBα, p- IKBα, P65, p-P65) of the NF-κB pathway. (k) Quantitative analysis of Western blot (n = 3). ANOVA followed by Bonferroni's multiple comparison test was used for statistical analysis (*p < 0.05, **p < 0.01, ***p < 0.001).

non-coding RNAs are present in Exos, particularly non-coding RNAs which are key mediators of cell-to-cell communication and possess potential therapeutic effects [39]. MicroRNAs (miRNAs) as small non-coding RNAs can coordinate several important molecular pathways orchestrating proliferation, apoptosis and inflammation [40]. The NF-κB pathway is a key regulator of the inflammatory response, especially, the receptor activator of NF-κB ligand that plays a major role in immune diseases affecting bone regeneration and is considered a critical factor that links the skeletal system to the immune system [41]. Exos has been demonstrated to negatively modulate the NF-κB pathway via miRNAs, such as miR199a, miR146, miR99a, miR181b, miR155 and miR411 leading to the inhibition of pro-inflammatory cytokines release [42]. The RT-qPCR result showed that the miRNAs, including miR199a, miR99a, miR146a, miR181a, and miR411, were expressed in the BMSC-derived Exos (Fig. S5a). After RAW264.7 cells ingested the Exos, the relative miRNAs were all increased in RAW264.7 cells, especially miR199a which increased by more than 2-fold (Fig. S5b). To further reveal the potential mechanisms of the osteoimmunomodulatory properties of Exo-loaded TA-SPEEK, the activation of the NF-κB pathway was investigated. The expression of phosphorylated IκB (*p*-IκB) was significantly down-regulated in the Exo-TA-SPEEK group compared to the other four groups (Fig. 3j and k). The *p*-IκB is the activator of the nuclear factor NF-κB, which plays a vital role in modulating the expression of pro-inflammatory genes [5]. As shown in Fig. 3j and k, protein phosphorylation degree of the downstream factors NF-κB p65 was also significantly down-regulated in the Exo-TA-SPEEK group. To further prove that Exos loaded SPEEK promoted macrophage M2 polarization via the NFκB pathway, we cultured RAW264.7 cells on Exo-coated TA-SPEEK and added the NF-κB pathway activator, LPS. As shown in Fig. S6, *p*-IKBα, p-P65 were significantly up-regulated, while IKBα was down-regulated in the LPS group when compared to the Exos loaded TA-SPEEK group. Together, these data indicate that Exo-coated TA-SPEEK may modulate macrophage polarization through downregulating the NF-κB pathway via miRNAs in Exos.

3.5. Promoting rat BMSCs differentiation by M2-polarized macrophages

To confirm that RAW264.7 cells did not differentiate into osteoclasts,
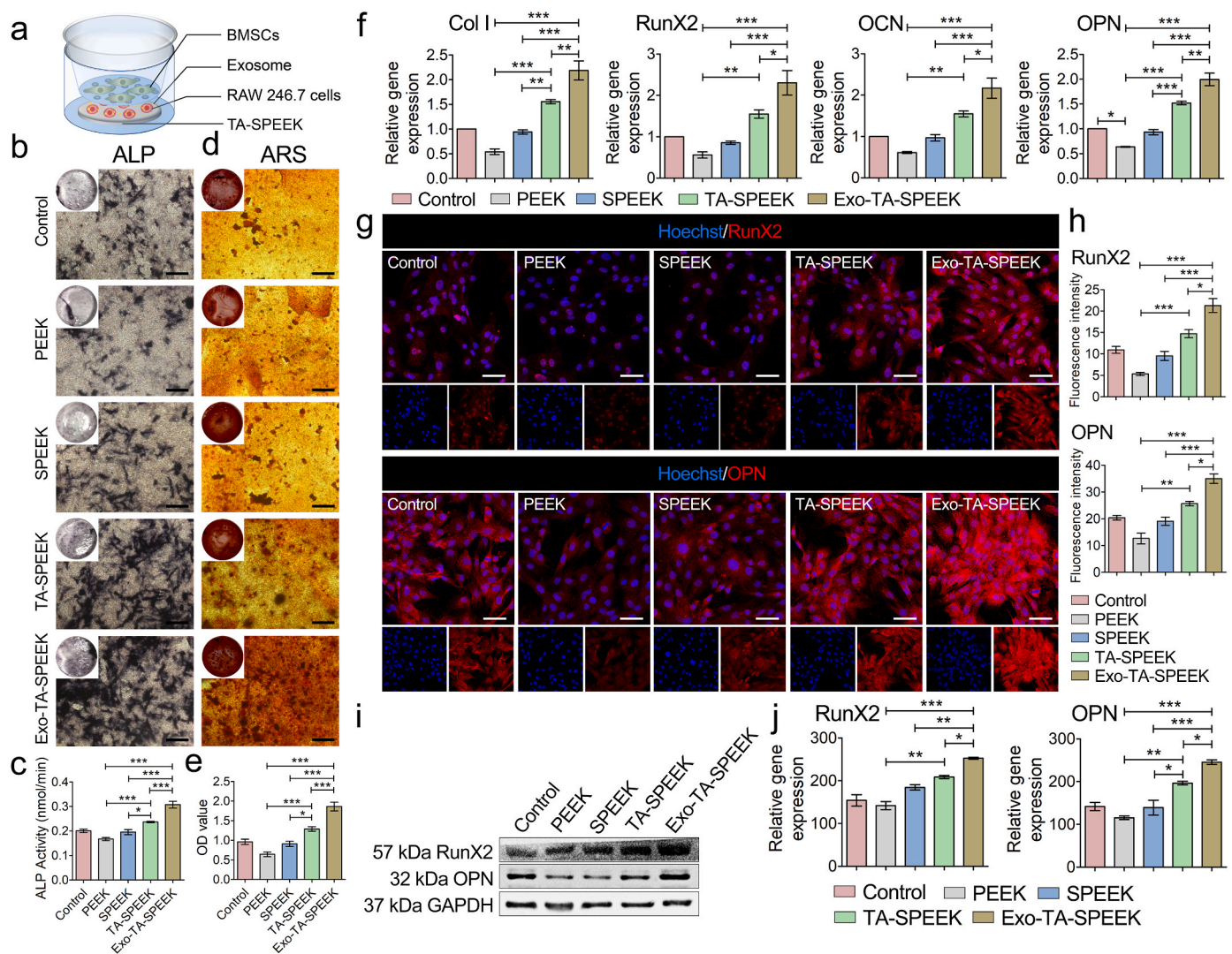
Fig. 4. Macrophage polarization effect on BMSCs osteogenesis. (a) A representative illustration of the co-culture system used. (b) ALP staining of BMSCs cultured for 7 days in a co-culture system. Scale bar represents 200 μm. (c) Quantitative analysis of ALP staining (n = 5). (d) ARS staining of BMSCs cultured for 7 days in the co-cultured system. Scale bar represents 200 μm. (e) Quantitative analysis of ARS staining (n = 5). (f) The expression of osteogenesis-related genes, such as Col I, RunX2, OCN, and OPN, was estimated by RT-qPCR after BMSCs co-culture for 7 days (n = 3). (g) RunX2 and OPN immunofluorescent staining of BMSCs was showed 7 days after being cultured in the co-culture system. RunX2 and OPN were stained red and the nuclei was stained blue. Scale bar represents 50 μm. (h) Quantitative analysis of immunofluorescent staining (n = 3). (i) The expression of RunX2 and OPN protein was evaluated by Western blot at 7 days. (j) Quantitative analysis of Western blot (n = 3). ANOVA followed by Bonferroni's multiple comparison test was used for statistical analysis (*p < 0.05, **p < 0.01, ***p < 0.001).

we used cytoskeleton staining and TRAP staining on day 1 and day 7 to evaluate the differentiation degree of the macrophages. As shown in Fig. S7, each group contained only a few cells with three or more nuclei or were stained dark red on day 7, suggesting that RAW264 did not differentiate into osteoclasts after 7 days of culture. To evaluate the osteoimmunomodulation effect on osteogenesis, the crosstalk between BMSCs and RAW264.7 cells was evaluated by a samples/RAW264.7 cells/BMSCs co-cultured system (Fig. 4a). The samples/BMSCs co-culture model was set as controls. After 7 days of co-culture, ALP staining and ARS were performed to assess osteogenic differentiation of the BMSCs. As previously reported, macrophages were recognized to balance the osteogenesis and osteoclastogenesis processes by regulating the molecules release [9]. Plenty of anti-inflammatory cytokines produced by M2 macrophages were known to induce osteogenesis [43]. Anti-inflammatory factors including IL-10, and TGFβ were found to prevent excessive inflammation and result in new bone tissue formation [44]. Exos promoted anti-inflammatory factors release, including Arg-1 and IL-10, which may induce BMSCs osteogenic differentiation. As shown in Fig. 4a, the highest ALP expression was detected in the Exo-coated TA-SPEEK group, followed by the TA-SPEEK, SPEEK, control and PEEK group (Fig. 4b and c). Similar to the trend of ALP staining, ARS

staining revealed that Exo-TA-SPEEK macrophage-conditioned medium significantly increased the mineralized nodules formation of BMSCs when compared to the other four groups (Fig. 4d and e). Meanwhile, BMSCs co-cultured with RAW264.7 cells on the Exo-coated SPEEK resulted in higher gene expression, including collagen I (Col I), Runx2, Osteopontin (OPN) and osteocalcin (OCN, Fig. 4f), and higher protein expression, including Runx2, OPN when compared to other four groups (Fig. 4g–j). These results showed that a more favorable environment for osteogenesis was constructed when immune cells were cultured on Exo-coated TA-SPEEK. On the contrary, ALP, ARS, and osteogenesis related gene and protein expression in PEEK groups were even lower than in the control group (Fig. 4b–j). It seemed that excessive inflammation inhibited osteogenic differentiation. Pro-inflammatory cytokines secreted by M1 macrophages may hinder the osteogenic gene expression of osteoblast-related cells [45]. TNF-a has been demonstrated to have an inhibitory effect on the expression of osteogenesis-related protein and mineralization of osteoblastic cells [3]. Due to highest M1 macrophage polarization and highest induction of pro-inflammatory cytokines, the osteogenic effect was lowest in the PEEK group. Here, we uncover Exos as a novel biocompatible coating that can provide a promising osteoimmunomodulatory environment to improve the bio-surface
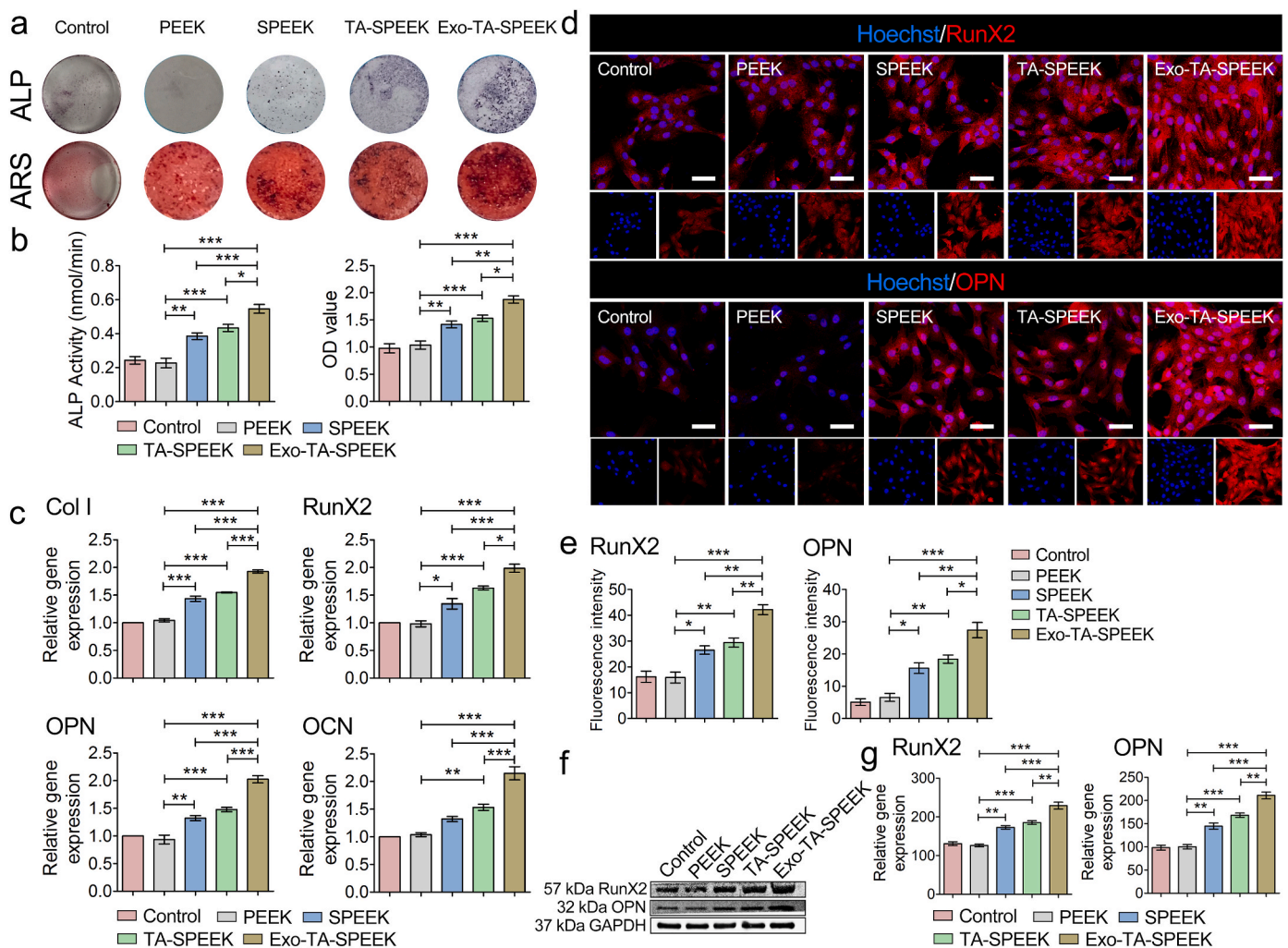
Fig. 5. Samples promoted osteogenic differentiation (a) ALP and ARS staining of BMSCs cultured for 7 days on the surface of the samples. (b) Quantitative analysis of ALP and ARS staining (n = 5). (c) Osteogenesis-related gene expression of BMSCs cultured on the surface of the samples at day 7 (Col I, RunX2, OCN, and OPN, n = 3). (d) RunX2 and OPN immunofluorescent staining of BMSCs was showed after 7 days cultured on the surface of the samples. RunX2 and OPN were stained red and the nuclei was stained blue. Scale bar represents 50 μm. (e) Quantitative analysis of immunofluorescent staining (n = 3). (f) The expression of RunX2 and OPN protein was evaluated by Western blot at 7 days. (g) Quantitative analysis of Western blot (n = 3). ANOVA followed by Bonferroni's multiple comparison test was used for statistical analysis (*p < 0.05, **p < 0.01, ***p < 0.001).

activities of PEEK resulting in enhanced osteogenic performance.

3.6. The direct osteogenic differentiation of BMSCs on different samples

The direct effect of the rough surface and Exos on the osteogenic differentiation of BMSCs were also evaluated. The surface roughness and hydrophilicity can enhance cell spreading, protein adsorption, and formation of bone-like matrix [18]. After 7 days of co-culture, ALP staining and ARS were performed to assess osteogenic differentiation of the BMSCs. ALP and ARS data showed that TA-SPEEK and SPEEK, which have a rougher surface, were more effective in stimulating the expression of ALP and mineralized nodules formation when compared to PEEK (Fig. 5a and b). Osteogenesis-related genes, such as Col I, RunX2, OPN, and OCN, and Osteogenesis-related proteins such as RunX2 and OPN were both higher in TA-SPEEK and SPEEK groups when compared to the PEEK group (Fig. 5c–g). It has been widely accepted that the rough surface of the materials is more beneficial for bone formation [24,46]. In addition, Exo-coated SPEEK exhibited the highest ALP expression and the most mineralized nodules formation (Fig. 5a and b). Similarly, additional Exos coated on the TA-SPEEK significantly promoted osteogenesis-related genes and proteins expressions when compared to the other four groups (Fig. 5c–g). Exos from the pre-differentiated BMSCs as a cell-free therapy have been demonstrated to promote the ALP activity and mineralization accumulation resulting in osteogenic differentiation of the BMSCs [14,16,47]. Exos containing various types

of non-coding RNA, especially miRNAs can modulate osteogenic differentiation of the BMSCs [48]. miRNAs, such as miR218, miR146a-5p, miR129-5p, miR483-3p, miR503-5p, can induce the osteogenic differentiation of BMSCs by activating the mitogen-activated protein kinase (MAPK) and phosphatidylinositol 3 kinase (PI3K)/Akt signaling pathway [16,47]. Herein, we found that surface chemistry together with Exos can exert a direct synergetic modulatory effect on bone formation. In conclusion, Exos simultaneously exerted direct bone formation property and osteoimmunomodulation effect which synergistically promote osteogenesis.

3.7. Results of in vivo rat air-pouch model

The *in vivo* immune response of each sample was measured using a rat air-pouch model [49]. Histological examinations, including HE, Masson's trichrome, and immunofluorescence, were performed to stain air-pouch tissue sections 7 days after sample implantation. HE staining and Masson's trichrome showed a thick continuous fibrous layer surrounding both PEEK (2120.56 ± 324.72 μm) and SPEEK (1900.50 ± 196.64 μm) implants, while the TA-SPEEK group showed a thinner fibrous layer (1263.01 ± 180.76 μm) which suggests lower *in vivo* inflammation (Fig. 6a and b). Exo-coated TA-SPEEK implants showed the thinnest fibrous layer (625.90 ± 132.86 μm), indicating the anti-inflammation properties of Exo-TA-SPEEK. Further, iNOS (M1 macrophages) and Arg-1 (M2 macrophages) immunofluorescence
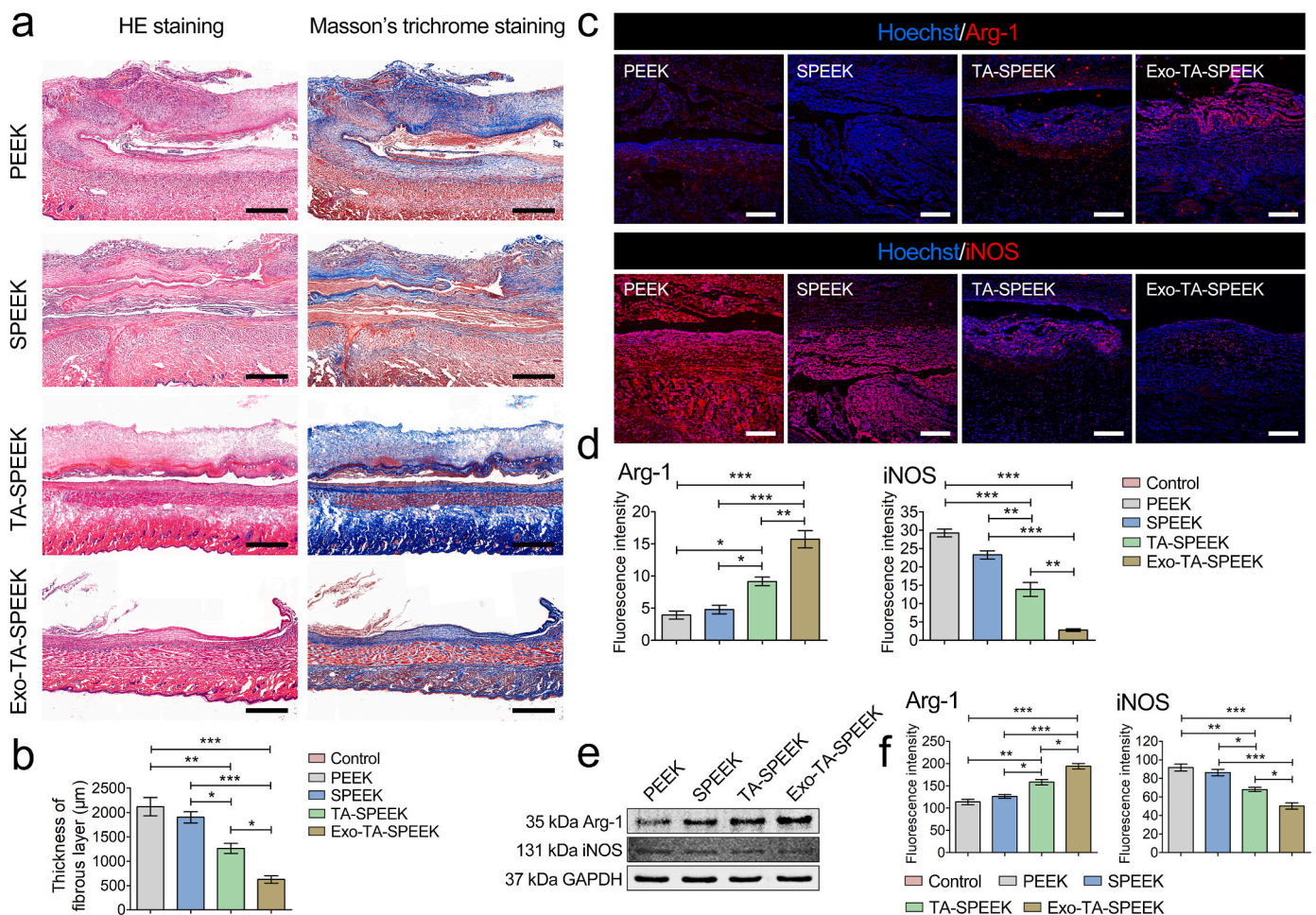
Fig. 6. Results of rat air-pouch model. (a) HE staining and Masson's trichrome staining of rat air-pouch skin. Scale bar represents 1 mm. (b) Quantitative analysis of the thickness of the fibrous layer (n = 3). (c) Immunofluorescent staining of Arg-1 and iNOS in air-pouch skin. Arg-1 and iNOS were stained red and the nuclei was stained blue. Scale bar represents 200 μm. (d) Quantitative analysis of immunofluorescent staining (n = 3). (e) The expression of Arg-1 and iNOS protein was evaluated by Western blot at 7 days. (f) Quantitative analysis of Western blot (n = 3). ANOVA followed by Bonferroni's multiple comparison test was used for statistical analysis (*p < 0.05, **p < 0.01, ***p < 0.001).

staining of fibrous layers revealed that more M1 macrophages and fewer M2 macrophages were present in PEEK and SPEEK groups when compared to the TA-SPEEK group (Fig. 6c and d). Addition of Exos in Exo-TA-SPEEK further increased the M2 macrophage proportion and inhibited M1 macrophage proportion when compared to TA-SPEEK group. Western blot results revealed that the trend of Arg-1 protein was Exo-TA-SPEEK > TA-SPEEK > SPEEK ≈ PEEK, while the trend of iNOS protein was the opposite: PEEK ≈ SPEEK > TA-SPEEK > Exo-TA-SPEEK (Fig. 6e and f). Therefore, the *in vivo* rat air-pouch model data were in accordance with the *in vitro* results demonstrating that Exo-coated TA-SPEEK can induce macrophage M2 polarization and produce an anti-inflammatory environment.

3.8. Results of in vivo new bone formation

The surgical procedure of sample implantation was shown in Fig. 7a. Eight weeks after the operation, the extracted femurs bone specimens were photographed by a photomicrograph system (Anyty) and evaluated by using a Micro-CT, which can provide both 2D and reconstructed 3D images and quantitative analyses data of newly regeneration bone. Micrographs showed that the obvious bone tissue healing was observed in the Exo-TA-SPEEK group (Fig. 7b). As the 2D images of the vertical sections of the samples show, the volume of new bone around the Exo-loaded TA-SPEEK was significantly higher than that around the other three implants as red arrows indicate (Fig. 7c). 3D reconstructed images showed a similar osteogenesis trend (Fig. 7d). Large amount of new bone
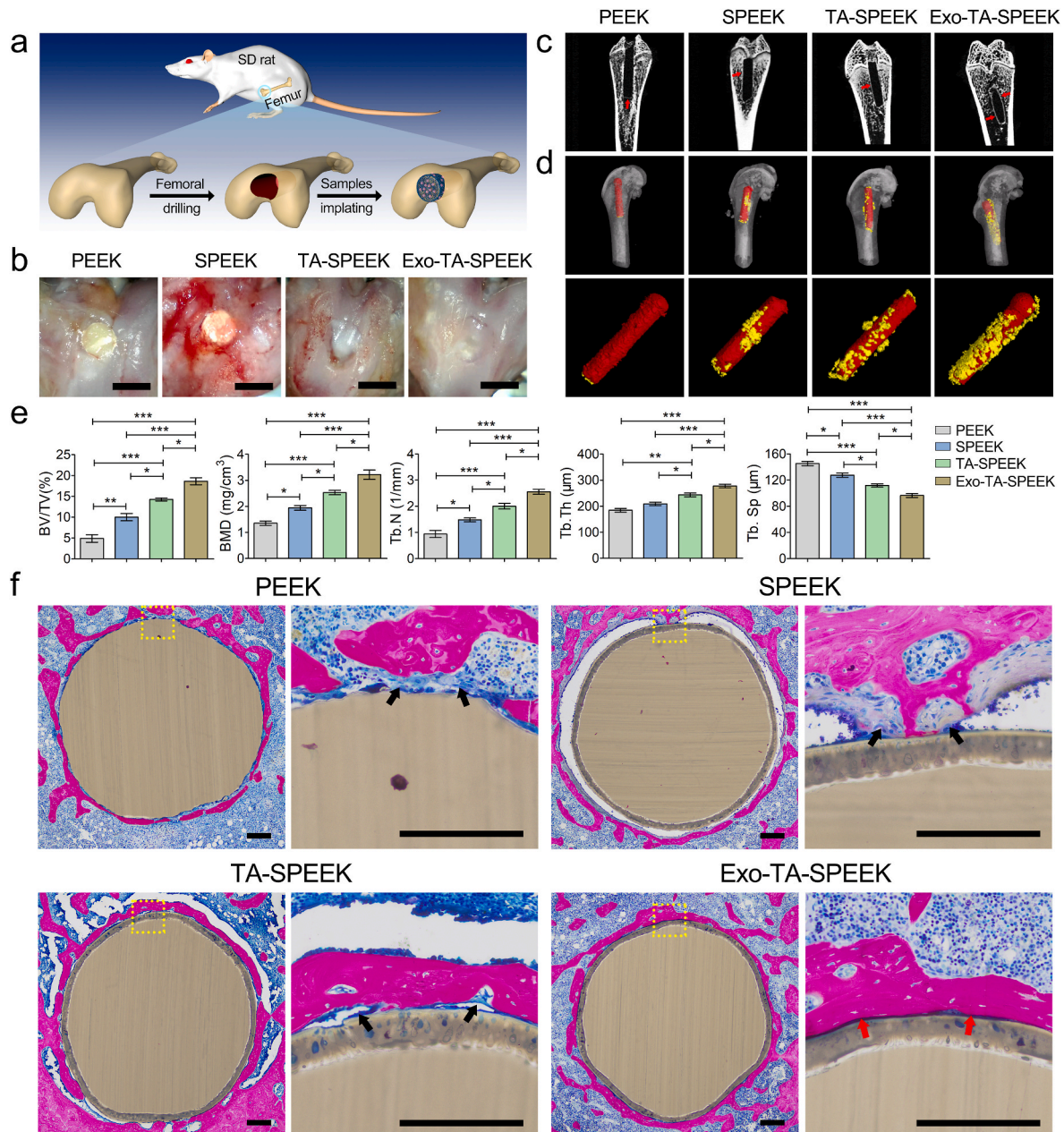
Fig. 7. *In vivo* new bone regeneration property of different implants. (a) An illustration of the rat femur surgical procedure. (b) General photos of the implantation site on the rat femur. Scale bar represents 2 mm. (c) Micro-CT images showing bone regeneration around the implants. The red arrows mark the new regeneration bone. (d) Reconstructed 3D images of samples and new bone. Yellow color indicates samples and red color indicates new regeneration bone. (e) Quantitative analysis of new bone 8 weeks after implantation (n = 3). (f) Histological images of methylene blue/acid fuchsin staining show the new regeneration bone around each sample 8 weeks post-operatively. Black arrow indicates collagen fiber formation. Red arrow indicates new bone formation. Scale bar represents 200 μm. ANOVA followed by Bonferroni's multiple comparison test was used for statistical analysis (*p < 0.05, **p < 0.01, ***p < 0.001).

was observed around Exo-TA-PEEK, while little bone was present around TA-SPEEK and SPEEK, and nearly no bone was found around PEEK. The quantitative analyses of new bone, including BV/TV, BMD, Tb.N, Tb.Th, and Tb.Sp are shown in Fig. 7e. The BV/TV, BMD, Tb.N, and Tb.Th were all highest in the Exo-TA-SPEEK group, followed by the TA-SPEEK and SPEEK groups and lowest in the PEEK group. Additionally, Exos coated TA-SPEEK implant showed the lowest Tb.Sp. Hence, Exo-loaded TA-SPEEK exerted the most positive effect on bone regeneration. Additionally, integration between implants and bone tissue was examined by methylene blue/acid fuchsin staining (Fig. 7f). The immune response plays a critical role in modulating the activities of tissue-resident cells, thereby regulating tissue regeneration [50]. Inappropriate immune reaction will lead to a chronic inflammation resulting in the fibrous encapsulation formation around the implant which ultimately caused osseointegration failure [3]. As the larger magnification image (Fig. S8a) shows, due to the excessive inflammation caused by untreated PEEK and SPEEK, histological staining revealed an obvious fibrous capsule indicated by the black arrow, which formed between the native bone and implants resulting in osseointegration failure. In contrast, no obvious fibrous formation was detected around Exo-TA-SPEEK implants. Moreover, Exo-loaded TA-SPEEK implants were tightly in contact with the newly regenerated bone, as indicated by the red arrow. For the TA-SPEEK group, although a lot of new regeneration bone bonded to the implants (red arrow), a few fibrous tissues were seen between the implants and newly formed bone (black arrow). A further quantitative analysis of the percentage of bone implant contact area also revealed that the bone implant contact of Exo-TA-SPEEK was significantly larger ($64.28 \pm 9.26\%$) than that of TA-SPEEK ($37.55 \pm 4.99\%$), SPEEK ($11.95 \pm 2.63\%$) and PEEK ($13.36 \pm 4.01\%$, $p < 0.001$, Fig. S8b). These findings are consistent with our *in vitro* results and further confirms that addition of Exos onto TA-SPEEK can significantly enhance osseointegration between the implant and the new bone *in vivo* mainly due to its osteoimmunomodulation properties.

4. Conclusion

In summary, BMSC-derived Exos were densely and uniformly deposited onto the TA-SPEEK surface and exhibited continuous and slow release from the TA-SPEEK for up to 14 days. Due to phagocytosis of Exos, BMSCs cultured on the Exo-TA-SPEEK showed better proliferation and adhesion abilities. Both *in vitro* and *in vivo* results revealed that Exo-loaded TA-SPEEK can modulate macrophages M2 polarization (an anti-inflammatory phenotype) via the NF-κB pathway. Furthermore, Exo-TA-SPEEK provides a more favorable bone immune microenvironment that is beneficial for further BMSCs osteogenic differentiation. In addition, our results showed that Exo-coated TA-SPEEK can promote the direct osteogenic differentiation of BMSCs. More importantly, our rat femoral drilling model demonstrates that Exo-TA-SPEEK implantation has immunomodulatory and direct osteogenic properties that can ultimately promote osseointegration and new bone formation *in vivo*. Altogether, we showed that Exos is an effective and potent additive to produce advanced immunomodulatory and bone regeneration materials.

CRediT authorship contribution statement

Lei Fan: Conceptualization, Methodology, Formal analysis, Validation, Investigation, Writing - original draft. **Pengfei Guan:** Methodology, Formal analysis, Validation. **Cairong Xiao:** Methodology, Validation, Formal analysis. **Huiquan Wen:** Visualization, Investigation. **Qiyou Wang:** Formal analysis, Funding acquisition, Visualization. **Can Liu:** Methodology, Validation. **Yian Luo:** Formal analysis, Investigation. **Limin Ma:** Methodology, Formal analysis. **Guoxin Tan:** Resources, Visualization. **Peng Yu:** Resources, Funding acquisition, Data curation. **Lei Zhou:** Conceptualization, Methodology, Funding acquisition, Writing - review & editing, Supervision, Data curation, Project administration. **Chengyun Ning:** Methodology, Funding acquisition,

Supervision.

Declaration of competing interest

The authors declare that they have no known competing financial interests or personal relationships that could have appeared to influence the work reported in this paper.

Appendix A. Supplementary data

Supplementary data to this article can be found online at https://doi.org/10.1016/j.bioactmat.2021.02.005.

References

[1] Z. Chen, A. Bachhuka, F. Wei, X. Wang, G. Liu, K. Vasilev, Y. Xiao, Nanotopography-based strategy for the precise manipulation of osteoimmunomodulation in bone regeneration, Nanoscale 9 (46) (2017) 18129–18152.

[2] W. Liu, J. Li, M. Cheng, Q. Wang, K.W.K. Yeung, P.K. Chu, X. Zhang, Zinc-modified sulfonated polyetheretherketone surface with immunomodulatory function for guiding cell fate and bone regeneration, Adv. Sci. (Weinheim, Baden-Wurttemberg, Germany) 5 (10) (2018) 1800749.

[3] Z. Chen, J. Yuen, R. Crawford, J. Chang, C. Wu, Y. Xiao, The effect of osteoimmunomodulation on the osteogenic effects of cobalt incorporated β-tricalcium phosphate, Biomaterials 61 (2015) 126–138.

[4] L. Chen, D. Wang, J. Qiu, X. Zhang, X. Liu, Y. Qiao, X. Liu, Synergistic effects of immunoregulation and osteoinduction of ds-block elements on titanium surface, Bioactive Mater. 6 (1) (2021) 191–207.

[5] Z. Chen, A. Bachhuka, S. Han, F. Wei, S. Lu, R.M. Visalakshan, K. Vasilev, Y. Xiao, Tuning chemistry and topography of nanoengineered surfaces to manipulate immune response for bone regeneration applications, ACS Nano 11 (5) (2017) 4494–4506.

[6] J. Li, W. Liu, D. Kilian, X. Zhang, M. Gelinsky, P.K. Chu, Bioinspired interface design modulates pathogen and immunocyte responses in biomaterial-centered infection combination therapy, Mater. Horizons (2019).

[7] A. Gao, Q. Liao, L. Xie, G. Wang, W. Zhang, Y. Wu, P. Li, M. Guan, H. Pan, L. Tong, P.K. Chu, H. Wang, Tuning the surface immunomodulatory functions of polyetheretherketone for enhanced osseointegration, Biomaterials 230 (2020) 119642.

[8] L. Chen, D. Wang, F. Peng, J. Qiu, L. Ouyang, Y. Qiao, X. Liu, Nanostructural surfaces with different elastic moduli regulate the immune response by stretching macrophages, Nano Lett. 19 (6) (2019) 3480–3489.

[9] J.M. Sadowska, F. Wei, J. Guo, J. Guillem-Marti, Z. Lin, M.P. Ginebra, Y. Xiao, The effect of biomimetic calcium deficient hydroxyapatite and sintered β-tricalcium phosphate on osteoimmune reaction and osteogenesis, Acta Biomater. 96 (2019) 605–618.

[10] Y. Shi, Y. Wang, Q. Li, K. Liu, J. Hou, C. Shao, Y. Wang, Immunoregulatory mechanisms of mesenchymal stem and stromal cells in inflammatory diseases, Nat. Rev. Nephrol. 14 (8) (2018) 493–507.

[11] P. Humbert, M. Brennan, N. Davison, P. Rosset, V. Trichet, F. Blanchard, P. Layrolle, Immune modulation by transplanted calcium phosphate biomaterials and human mesenchymal stromal cells in bone regeneration, Front. Immunol. 10 (2019) 663.

[12] M. Brennan, P. Layrolle, D.J. Mooney, Biomaterials functionalized with MSC secreted extracellular vesicles and soluble factors for tissue regeneration, Adv. Funct. Mater. 30 (37) (2020).

[13] L. Li, Y. Zhang, J. Mu, J. Chen, C. Zhang, H. Cao, J. Gao, Transplantation of human mesenchymal stem-cell-derived exosomes immobilized in an adhesive hydrogel for effective treatment of spinal cord injury, Nano Lett. 20 (6) (2020) 4298–4305.

[14] J. Fan, C.S. Lee, S. Kim, C. Chen, T. Aghaloo, M. Lee, Generation of small RNA-modulated exosome mimetics for bone regeneration, ACS Nano 14 (9) (2020) 11973–11984.

[15] W. Liu, Y. Rong, J. Wang, Z. Zhou, X. Ge, C. Ji, D. Jiang, F. Gong, L. Li, J. Chen, S. Zhao, F. Kong, C. Gu, J. Fan, W. Cai, Exosome-shuttled miR-216a-5p from hypoxic preconditioned mesenchymal stem cells repair traumatic spinal cord injury by shifting microglial M1/M2 polarization, J. Neuroinflammation 17 (1) (2020) 47.

[16] M. Zhai, Y. Zhu, M. Yang, C. Mao, Human mesenchymal stem cell derived exosomes enhance cell-free bone regeneration by altering their miRNAs profiles, Adv. Sci. (Weinheim, Baden-Wurttemberg, Germany) 7 (19) (2020) 2001334.

[17] X. Yuan, L. Ouyang, Y. Luo, Z. Sun, C. Yang, J. Wang, X. Liu, X. Zhang, Multifunctional sulfonated polyetheretherketone coating with beta-defensin-14 for yielding durable and broad-spectrum antibacterial activity and osseointegration, Acta Biomater. 86 (2019) 323–337.

[18] Y. Zhao, H.M. Wong, S.C. Lui, E.Y. Chong, G. Wu, X. Zhao, C. Wang, H. Pan, K. M. Cheung, S. Wu, P.K. Chu, K.W. Yeung, Plasma surface functionalized polyetheretherketone for enhanced osseo-integration at bone-implant interface, ACS Appl. Mater. Interfaces 8 (6) (2016) 3901–3911.

[19] X. Xu, Y. Li, L. Wang, Y. Li, J. Pan, X. Fu, Z. Luo, Y. Sui, S. Zhang, L. Wang, Y. Ni, L. Zhang, S. Wei, Triple-functional polyetheretherketone surface with enhanced bacteriostasis and anti-inflammatory and osseointegrative properties for implant application, Biomaterials 212 (2019) 98–114.

[20] L. He, T. He, J. Xing, Q. Zhou, L. Fan, C. Liu, Y. Chen, D. Wu, Z. Tian, B. Liu, L. Rong, Bone marrow mesenchymal stem cell-derived exosomes protect cartilage damage and relieve knee osteoarthritis pain in a rat model of osteoarthritis, Stem Cell Res. Ther. 11 (1) (2020) 276.

[21] J. Choi, Y. Chen, R. Abbel, I. Visagie, K. Parker, Flexible humidity sensors for wireless monitoring based on electrospun sulfonated polyether ether ketone (SPEEK) nanofibres, Sensor. Actuator. B Chem. 324 (2020).

[22] N.T. Evans, F.B. Torstrick, C.S. Lee, K.M. Dupont, D.L. Safranski, W.A. Chang, A. E. Macedo, A.S. Lin, J.M. Boothby, D.C. Whittingslow, R.A. Carson, R.E. Guldberg, K. Gall, High-strength, surface-porous polyether-ether-ketone for load-bearing orthopedic implants, Acta Biomater. 13 (2015) 159–167.

[23] J. Yan, W. Zhou, Z. Jia, P. Xiong, Y. Li, P. Wang, Q. Li, Y. Cheng, Y. Zheng, Endowing polyetheretherketone with synergistic bactericidal effects and improved osteogenic ability, Acta Biomater. 79 (2018) 216–229.

[24] Y. Zhao, H.M. Wong, W. Wang, P. Li, Z. Xu, E.Y. Chong, C.H. Yan, K.W. Yeung, P. K. Chu, Cytocompatibility, osseointegration, and bioactivity of three-dimensional porous and nanostructured network on polyetheretherketone, Biomaterials 34 (37) (2013) 9264–9277.

[25] X. Qi, Y. Hou, M. Yang, Scalable synthesis of multifunctional epidermis-like smart coatings, Adv. Funct. Mater. 29 (36) (2019) 1903984.1–1903984.12.

[26] R. Xu, S. Ma, P. Lin, B. Yu, F. Zhou, W. Liu, High strength astringent hydrogels using protein as the building block for physically cross-linked multi-network, ACS Appl. Mater. Interfaces 10 (9) (2018) 7593–7601.

[27] S. Kim, D.S. Kim, S.M. Kang, Reversible layer-by-layer deposition on solid substrates inspired by mussel byssus cuticle, Chem. Asian J. 9 (1) (2014) 63–66.

[28] F. Behboodi-Sadabad, H. Zhang, V. Trouillet, A. Welle, N. Plumere, P.A. Levkin, UV-Triggered polymerization, deposition, and patterning of plant phenolic compounds, Adv. Funct. Mater. 27 (22) (2017) 1700127.1–1700127.11.

[29] Z. Zhao, D.C. Pan, Q.M. Qi, J. Kim, N. Kapate, T. Sun, C.W.t. Shields, L.L. Wang, D. Wu, C.J. Kwon, W. He, J. Guo, S. Mitragotri, Engineering of Living Cells with Polyphenol-Functionalized Biologically Active Nanocomplexes, Advanced Materials, Deerfield Beach, Fla., 2020, e2003492.

[30] Z. Zeng, K. Pu, Improving cancer immunotherapy by cell membrane-camouflaged nanoparticles, Adv. Funct. Mater. 30 (43) (2020) 2004397.

[31] X. Zhen, P. Cheng, K. Pu, Recent advances in cell membrane-camouflaged nanoparticles for cancer phototherapy, Small 15 (1) (2019), e1804105.

[32] J. Li, X. Zhen, Y. Lyu, Y. Jiang, J. Huang, K. Pu, Cell membrane coated semiconducting polymer nanoparticles for enhanced multimodal cancer phototheranostics, ACS Nano 12 (8) (2018) 8520–8530.

[33] W. Liu, J. Li, M. Cheng, Q. Wang, Y. Qian, K.W.K. Yeung, P.K. Chu, X. Zhang, A surface-engineered polyetheretherketone biomaterial implant with direct and immunoregulatory antibacterial activity against methicillin-resistant Staphylococcus aureus, Biomaterials 208 (2019) 8–20.

[34] X. Wang, F.A. Shah, F. Vazirisani, A. Johansson, A. Palmquist, O. Omar, K. Ekström, P. Thomsen, Exosomes influence the behavior of human mesenchymal stem cells on titanium surfaces, Biomaterials 230 (2020) 119571.

[35] S. Zhang, S.J. Chuah, R.C. Lai, J.H.P. Hui, S.K. Lim, W.S. Toh, MSC exosomes mediate cartilage repair by enhancing proliferation, attenuating apoptosis and modulating immune reactivity, Biomaterials 156 (2018) 16–27.

[36] S.S. Jin, D.Q. He, D. Luo, Y. Wang, M. Yu, B. Guan, Y. Fu, Z.X. Li, T. Zhang, Y. H. Zhou, C.Y. Wang, Y. Liu, A biomimetic hierarchical nanointerface orchestrates macrophage polarization and mesenchymal stem cell recruitment to promote endogenous bone regeneration, ACS Nano 13 (6) (2019) 6581–6595.

[37] C. Yang, L. Ouyang, W. Wang, B. Chen, W. Liu, X. Yuan, Y. Luo, T. Cheng, K.W. K. Yeung, X. Liu, X. Zhang, Sodium butyrate-modified sulfonated polyetheretherketone modulates macrophage behavior and shows enhanced antibacterial and osteogenic functions during implant-associated infections, J. Mater. Chem. B 7 (36) (2019) 5541–5553.

[38] L. Zhou, L. Fan, X. Yi, Z. Zhou, C. Liu, R. Fu, C. Dai, Z. Wang, X. Chen, P. Yu, D. Chen, G. Tan, Q. Wang, C. Ning, Soft conducting polymer hydrogels cross-linked and doped by tannic acid for spinal cord injury repair, ACS Nano 12 (11) (2018) 10957–10967.

[39] W. Duan, W. Zhang, J. Jia, Q. Lu, M. Eric Gershwin, Exosomal microRNA in autoimmunity, Cell. Mol. Immunol. 16 (12) (2019) 932–934.

[40] M. Ghibaudi, M. Boido, A. Vercelli, Functional integration of complex miRNA networks in central and peripheral lesion and axonal regeneration, Prog. Neurobiol. 158 (2017) 69–93.

[41] K. Okamoto, T. Nakashima, M. Shinohara, T. Negishi-Koga, N. Komatsu, A. Terashima, S. Sawa, T. Nitta, H. Takayanagi, Osteoimmunology: the conceptual framework unifying the immune and skeletal systems, Physiol. Rev. 97 (4) (2017) 1295–1349.

[42] K. Taniguchi, M. Karin, NF-κB, inflammation, immunity and cancer: coming of age, Nat. Rev. Immunol. 18 (5) (2018) 309–324.

[43] J.M. Sadowska, F. Wei, J. Guo, J. Guillem-Marti, M.P. Ginebra, Y. Xiao, Effect of nano-structural properties of biomimetic hydroxyapatite on osteoimmunomodulation, Biomaterials 181 (2018) 318–332.

[44] G. Liu, X. Wang, X. Zhou, L. Zhang, J. Mi, Z. Shan, B. Huang, Z. Chen, Z. Chen, Modulating the cobalt dose range to manipulate multisystem cooperation in bone environment: a strategy to resolve the controversies about cobalt use for orthopedic applications, Theranostics 10 (3) (2020) 1074–1089.

[45] Q.L. Ma, L. Fang, N. Jiang, L. Zhang, Y. Wang, Y.M. Zhang, L.H. Chen, Bone mesenchymal stem cell secretion of sRANKL/OPG/M-CSF in response to macrophage-mediated inflammatory response influences osteogenesis on nanostructured Ti surfaces, Biomaterials 154 (2018) 234–247.

[46] B. Huang, L. Tan, X. Liu, J. Li, S. Wu, A facile fabrication of novel stuff with antibacterial property and osteogenic promotion utilizing red phosphorus and near-infrared light, Bioactive Mater. 4 (1) (2019) 17–21.

[47] W. Li, Y. Liu, P. Zhang, Y. Tang, M. Zhou, W. Jiang, X. Zhang, G. Wu, Y. Zhou, Tissue-Engineered bone immobilized with human adipose stem cells-derived exosomes promotes bone regeneration, ACS Appl. Mater. Interfaces 10 (6) (2018) 5240–5254.

[48] S. Zhu, F. Yao, H. Qiu, G. Zhang, H. Xu, J. Xu, Coupling factors and exosomal packaging microRNAs involved in the regulation of bone remodelling, Biol. Rev. Camb. Phil. Soc. 93 (1) (2018) 469–480.

[49] P.K. Gavel, H.S. Parmar, V. Tripathi, N. Kumar, A. Biswas, A.K. Das, Investigations of anti-inflammatory activity of a peptide-based hydrogel using rat air pouch model, ACS Appl. Mater. Interfaces 11 (3) (2019) 2849–2859.

[50] J. Yan, D. Xia, W. Zhou, Y. Li, P. Xiong, Q. Li, P. Wang, M. Li, Y. Zheng, Y. Cheng, pH-responsive silk fibroin-based CuO/Ag micro/nano coating endows polyetheretherketone with synergistic antibacterial ability, osteogenesis, and angiogenesis, Acta Biomater. 115 (2020) 220–234.